Chemical Science

ROYAL SOCIETY OF CHEMISTRY

EDGE ARTICLE

View Article Online
View Journal | View Issue

Cite this: *Chem. Sci.*, 2024, **15**, 16559

All publication charges for this article have been paid for by the Royal Society of Chemistry

Received 22nd July 2024
Accepted 4th September 2024

DOI: 10.1039/d4sc04880f

rsc.li/chemical-science

A homoleptic Fe(IV) ketimide complex with a low-lying excited state†

Phoebe R. Hertler,[a] Arturo Sauza-de la Vega,[b] Andrea Darù,[b] Arup Sarkar,[b] Richard A. Lewis,[a] Guang Wu,[a] Laura Gagliardi*[b] and Trevor W. Hayton*[a]

The reaction of 4 equiv. of Li(N=C(^{t}Bu)Ph) with $Fe^{II}Cl_2$ results in isolation of $[Li(Et_2O)]_2[Fe^{II}(N{=}C(^t Bu)Ph)_4]$ (**1**), in good yields. The reaction of **1** with 1 equiv. of I_2 leads to formation of $[Fe^{IV}(N{=}C(^t Bu)Ph)_4]$ (**2**), in moderate yields. ^{57}Fe Mössbauer spectroscopy confirms the Fe(IV) oxidation state of **2**, and X-ray crystallography reveals that **2** has a square planar coordination geometry along with several intramolecular H···C interactions. Furthermore, SQUID magnetometry indicates a small magnetic moment at room temperature, suggestive of an accessible $S = 1$ state. Both density functional theory and multiconfigurational calculations were done to elucidate the nature of the ground state. Consistent with the experimental results, the ground state was found to be an $S = 0$ state with an $S = 1$ excited state close in energy.

Introduction

In comparison to the oxo, nitrido, and imido chemistry of Fe(IV),[1–18] the coordination and organometallic chemistry of this oxidation state is relatively sparse.[19–33] The paucity of examples is generally ascribed to the high oxidizing power of Fe^{4+}, which can oxidize sensitive organometallic ligands.[11,34–38] As a result, many of the Fe(IV) coordination complexes isolated thus far contain additional stabilizing features. For example, London dispersion forces are thought to play an important role in the stability of $[Fe^{IV}(1\text{-norbornyl})_4]$ and $[Fe^{IV}(\text{cyclohexyl})_4]$.[39–42] Likewise, the solid-state structure of $[Fe^{IV}(C_5Me_5)_2][SbF_6]_2$ displays multiple close contacts between the methyl groups of the cation and fluorine atoms of the anions.[24] In contrast, the homoleptic Fe(IV) ketimide complex, $[Fe^{IV}(N{=}C^tBu_2)_4]$,[27] acquires its stability *via* the exceptionally strong σ- and π-donor properties of the ketimide ligand.[43–45] In fact, the di-*tert*-butyl ketimide ligand can stabilize a large series of homoleptic M(IV) complexes of the type $[M^{IV}(N{=}C^tBu_2)_4]$ (M = Ti, V, Nb, Ta, Cr, Mo, W, Mn, Fe, Co).[27,44–49] This ligand also stabilizes the U^{5+} ion in the homoleptic penta(ketimide) complex, $[U^{V}(N{=}C^tBu_2)_5]$,[50] while the closely related phenyl-*tert*-butyl ketimide, $[N{=}C(^tBu)Ph]^-$, can stabilize U(VI) and Ce(IV) – two ions that are also considered a challenge to isolate.[50,51] Similarly, the stability of $[Fe^{IV}(mnt)_3]^{2-}$ (mnt = maleonitriledithiolate) was thought to be due to highly covalent π-interaction between the Fe^{4+} centers and the $[mnt]^{2-}$ ligand.[25]

Given the paucity of Fe(IV) coordination complexes, we have continued to explore the chemistry of high-valent iron ketimides. Herein, we report the synthesis of unusual square planar, homoleptic Fe(IV) ketimide complex, $[Fe^{IV}(N{=}C(^tBu)Ph)_4]$, which features a singlet ($S = 0$) ground state. However, NMR spectral data, magnetism measurements, and density functional theory (DFT) and multiconfigurational calculations support the presence of a low-lying triplet state that is partially populated at room temperature.

Results and discussion

The reaction of $Fe^{II}Cl_2$ with 4 equiv. of Li(N=C(^{t}Bu)Ph) results in formation of $[Li(Et_2O)]_2[Fe^{II}(N{=}C(^tBu)Ph)_4]$ (**1**), which crystallizes from a mixture of pentane and Et_2O as large, orange blocks in 76% yield after work-up (Scheme 1). Complex **1** crystallizes in the monoclinic space group $P2_1/c$ and features a distorted tetrahedral environment about the Fe center (Fig. 1). Additionally, the two Li^+ cations are bound to two ketimide N atoms and one Et_2O molecule. Similar structural features are found in the related homoleptic Fe(II) ketimide complexes, $[Li(THF)]_2[Fe^{II}(N{=}C^tBu_2)_4]$ and $[Li(THF)_2]_2[Fe^{II}(N{=}C_{13}H_8)_4]$.[27,52] The Fe–N distances in **1** range from 2.043(4) to 2.056(4) Å and are comparable to those observed for other Fe(II) ketimide complexes.[27,52] Its ^{1}H NMR spectrum in THF-d_8 features a broad, paramagnetically shifted resonance at 16.0 ppm, assignable to the ^{t}Bu environment, as well as broad

[a]*Department of Chemistry and Biochemistry, University of California Santa Barbara, Santa Barbara, CA 93106, USA. E-mail: hayton@chem.ucsb.edu*

[b]*Department of Chemistry, Pritzker School of Molecular Engineering, James Franck Institute, University of Chicago, Chicago, IL 60637, USA. E-mail: lgagliardi@uchicago.edu*

† Electronic supplementary information (ESI) available: Experimental procedures and crystallographic, spectroscopic, electrochemical, and magnetic characterization details for **1** and **2** (PDF and CIF files). CCDC 2254712, 2254713 and 2363649. For ESI and crystallographic data in CIF or other electronic format see DOI: https://doi.org/10.1039/d4sc04880f

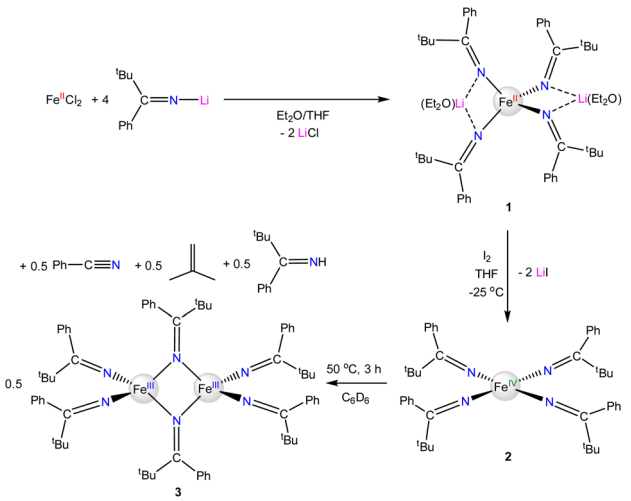

Scheme 1 Synthesis of complexes **1–3**.

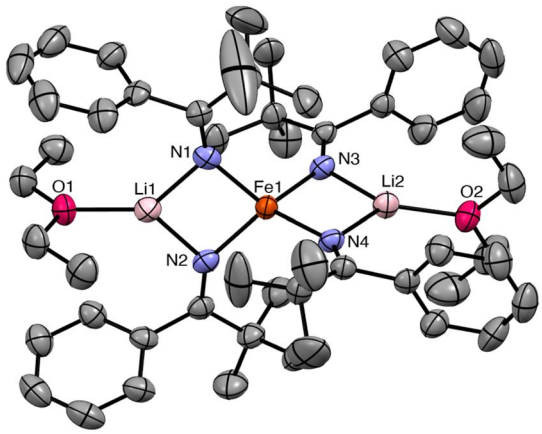

Fig. 1 Solid-state structure of $[Li(Et_2O)]_2[Fe(N{=}C(^tBu)Ph)_4]$ (**1**) with 50% probability ellipsoids. Hydrogen atoms have been omitted for clarity. Selected bond lengths (Å) and angles (°): Fe1–N1 = 2.051(4), Fe1–N2 = 2.056(4), Fe1–N3 = 2.045(4), Fe1–N4 = 2.043(4), N1–Fe1–N3 = 114.00(14), N1–Fe1–N2 = 93.21(14), and N1–Fe1–N4 = 121.09(14).

resonances at 12.7 and 7.87 ppm, assignable to the *o*/*m* phenyl environments (Fig. S2†). Additionally, its $^7Li\{^1H\}$ NMR spectrum consists of an extremely broad, paramagnetically shifted resonance at 391 ppm (Fig. S3†), suggesting the presence of a contact-ion pair in solution. Similar behavior is observed in other $[Li]_2[M^{II}(ketimide)_4]$-type complexes.[27,44,47,52]

The reaction of **1** with 1 equiv. of I_2 results in formation of $[Fe^{IV}(N{=}C(^tBu)Ph)_4]$ (**2**), which can be isolated as black crystals in 32% yield after work-up (Scheme 1). Interestingly, we also observe formation of the previously reported Fe(III) complex, $[Fe^{III}{}_2(N{=}C(^tBu)Ph)_6]$ (**3**),[52] during the oxidation of **1** to **2** (Fig. S10†), which is presumably formed by over-oxidation of **1** and which helps account for the low isolated yields of **2**. Complex **2** can also be generated *via* oxidation of **1** with 1.7 equiv. of $AgPF_6$ or 1.7 equiv. of $[Cp_2Fe][BF_4]$; however, neither reaction is synthetically useful. In the case of $AgPF_6$, several byproducts are formed, including **3**, despite the use of substoichiometric quantities of $AgPF_6$. The oxidation of **1** with $[Cp_2Fe][BF_4]$ is relatively clean, but complex **2** proved too difficult to separate from the $[Cp_2Fe]$ by-product, due to their similar solubilities.

Complex **2** crystallizes from Et_2O and hexanes in the monoclinic space group *C*2/*c* (Fig. 2). In the solid state, **2** exhibits a distorted square planar geometry (τ_4 = 0.19),[53] wherein all four phenyl rings point up and all four ^{t}Bu groups point down. Complex **2** features a nearly linear N1–Fe1–N1* angle (172.96(10)°). However, the N2–Fe1–N2* angle is notably smaller (159.70(10)°) and the Fe–N–C angle of these two ketimide ligands also deviates from linearity (Fe–N2–C12 = 149.24(14)°). This distortion is attributable to the presence of short inter-ligand H···C contacts. In particular, H22 is in close proximity to both C6 and C11 (H22···C6 = 2.726 Å and H22···

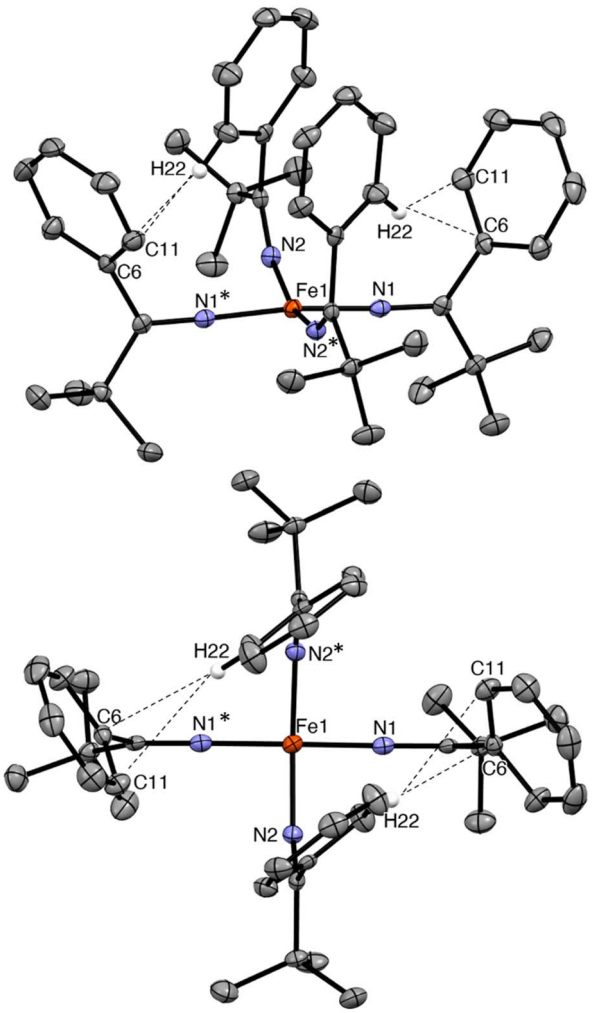

Fig. 2 Two views of the solid-state molecular structure of $[Fe(N{=}C(^tBu)Ph)_4]$ (**2**) measured at 100 K, shown with 50% probability ellipsoids. Hydrogen atoms (except H22) have been omitted for clarity. Selected bond lengths (Å) and angles (°): Fe1–N1 = 1.7571(17), Fe1–N2 = 1.7859(15), N1–Fe1–N2 = 90.26(7), N1–Fe–N2* = 90.99(7), N1–Fe1–N1* = 172.96(10), N2–Fe1–N2* = 159.70(10), Fe1–N1–C1 = 177.62(16), and Fe1–N2–C12 = 149.24(14).

C11 = 2.900 Å, Fig. 2), distances that are within the sum of their van der Waals radii ($r_H r_C$ = 2.9 Å).[41,54] These interactions may contribute to the overall stability of the complex, as has been noted for other Fe(IV) coordination and organometallic complexes,[39–42] as well as the observed syn arrangement of the phenyl groups. Finally, the Fe–N distances in **2** are 1.7571(17) and 1.7859(15) Å. These values are similar to those previously reported for $[Fe^{IV}(N{=}C^tBu_2)_4]$ (1.771(3) and 1.775(3) Å) and are somewhat shorter than Fe–N distances in $[Fe^{IV}(TAML)(CN)_2][PPh_4]_2$ (1.807(9)–1.950(9) Å),[32] $[(N_3N')Fe^{IV}(CN)]$ (av. 1.82 Å),[19] and $[Fe(MesNCH_2CH_2NMes)_2]$ (av. 1.89 Å).[33] The latter complex also exhibits a distorted square planar geometry (τ_4 = 0.22). Finally, the metrical parameters of a crystal of **2**, collected at 287(2) K, are nearly identical to those collected at 100(2) K (Table S2†), demonstrating that the square planar geometry is maintained at room temperature in the solid state.

The ^{1}H NMR spectrum of **2** in toluene-d_8 exhibits four paramagnetically shifted resonances at 8.92, 7.70, 5.33, and 2.68 ppm in a 2 : 2: 1 : 9 ratio, which are assignable to the *m*-Ar, *o*-Ar, *p*-Ar, and ^{t}Bu protons, respectively. The *o*-Ar resonance is notably broad, likely because of the aforementioned H···C contacts, demonstrating that these interactions are probably maintained in solution. These resonances shift upon cooling. For example, at −60 °C in toluene-d_8, the *m*-Ar resonance at 8.92 ppm shifts upfield to 7.37 ppm, whereas the *p*-Ar resonance at 5.33 ppm shifts downfield to 6.42 ppm (Fig. S6 and S7†). The shift of the ^{1}H resonances upon cooling is not consistent with temperature-independent paramagnetism (TIP),[55] but is instead the result of a thermally populated low-lying electronic excited state (see below).[56,57] In contrast, $[Fe^{IV}(N{=}C^tBu_2)_4]$ is diamagnetic at room temperature, indicating the difference in the electronic structure imparted by the stronger donating bis(*tert*-butyl) ketimide ligand. For further comparison, the recently reported $[Fe(MesNCH_2CH_2NMes)_2]$ exhibits an S = 1 ground state at room temperature, suggesting that the bis(amide) ligand is a weaker donor than $[N{=}C(^tBu)Ph]^-$.[33]

Complex **2** is soluble in hexanes, benzene, Et_2O, and THF. It is stable as a solid for two weeks under an inert atmosphere at −25 °C; however, at longer storage times, it begins to decompose into the previously reported Fe(III) complex, **3**.[52] Complex **2** is also unstable in solution. Thermolysis of **2** for 3 h at 50 °C in C_6D_6, results in complete conversion to **3**, according to ^{1}H and ^{13}C NMR spectroscopy (Scheme 1, Fig. S13 and S14†).[52] Also present in these spectra are signals attributable to PhCN, isobutylene, and $HN{=}C(^tBu)Ph$, which are present in an approximately 1 : 1 : 1 ratio. These products are apparently derived from the one-electron oxidation of the ketimide ligand by the Fe(IV) center.[47,48] For comparison, $[Fe^{IV}(N{=}C^tBu_2)_4]$ also decomposes upon heating in C_6D_6 forming $[Fe_2(N{=}C^tBu_2)_5]$, *tert*-butyl cyanide, isobutane, and isobutylene;[48] however, its complete conversion required 8 h at 50 °C, suggesting that the $[N{=}C(^tBu)Ph]^-$ ligand is more easily oxidized. Finally, the reaction of **2** with $HN{=}CPh_2$ in an attempt to form $[Fe^{IV}(N{=}CPh_2)_4]$ results in the formation of $[Fe^{III}{}_2(N{=}CPh_2)_6]$,[52] along with isobutylene, PhCN, and $HN{=}C^tBuPh$ (Scheme S1 and Fig. S15†). This observation indicates that the diphenyl ketimide ligand is likely unable to support the Fe(IV) state.

The cyclic voltammogram of **2** in THF reveals two reversible redox events, with $E_{1/2}$ values of −1.40 and −0.36 V (*vs.* Fc/Fc^+) (Fig. S20†). The former is attributed to the Fe(II)/Fe(III) redox couple, and the latter is attributed to the Fe(III)/Fe(IV) redox couple. For comparison, $[Fe^{IV}(N{=}C^tBu_2)_4]$ features an Fe(II)/Fe(III) redox couple at −1.63 V and an Fe(III)/Fe(IV) redox couple at −0.53 V (*vs.* Fc/Fc^+).[27] The *ca.* 0.2 V shift in potential for **2** is unsurprising, given that phenyl ligands are less electron-donating than *tert*-butyl groups.[58]

The zero-field ^{57}Fe Mössbauer spectrum for **2** at 90 K displays a doublet with δ = −0.162(2) mm s^{-1} and $|\Delta E_Q|$ = 1.837(3) mm s^{-1} (Fig. 3 and Table 1). The isomer shift is very similar to those reported for $[Fe^{IV}(N{=}C^tBu_2)_4]$ (δ = −0.15 mm s^{-1}) and $[Fe(MesNCH_2CH_2NMes)_2]$ (δ = −0.15 mm s^{-1}),[33,48] as well as other Fe(IV) complexes,[2,7,8,48,59] corroborating the proposed +4 oxidation state assignment. For further comparison, the Mössbauer spectrum of **1** exhibits a much larger isomer shift (δ = 0.924(2) mm s^{-1}; Fig. S19†), consistent with its lower oxidation state. Interestingly, the zero-field ^{57}Fe Mössbauer spectrum for **2**, collected at 298 K, displays a similar isomer shift (−0.096(4) mm s^{-1})[60] but much smaller quadrupolar splitting ($|\Delta E_Q|$ = 1.172(7) mm s^{-1}) (Fig. 3), suggesting a decrease in the electric field gradient with increasing temperature.[61]

Temperature-dependent dc magnetization data were collected for a crystalline sample of **2** at H = 1000 Oe, revealing a linear increase in $\chi_M T$ from 0.00 cm^3 K mol^{-1} (μ_{eff} = 0.08 μ_B) at T = 2 K to 0.17 cm^3 K mol^{-1} (μ_{eff} = 1.17 μ_B) at T = 300 K (Fig. 4). These results indicate that, at very low temperatures, **2** has a singlet spin ground state (S = 0). However, at room temperature, the moment is still well below that expected for an S = 1 system (1.00 cm^3 K mol^{-1}). To explain this data, we hypothesize that a low-lying excited state is partially populated as the temperature increases.

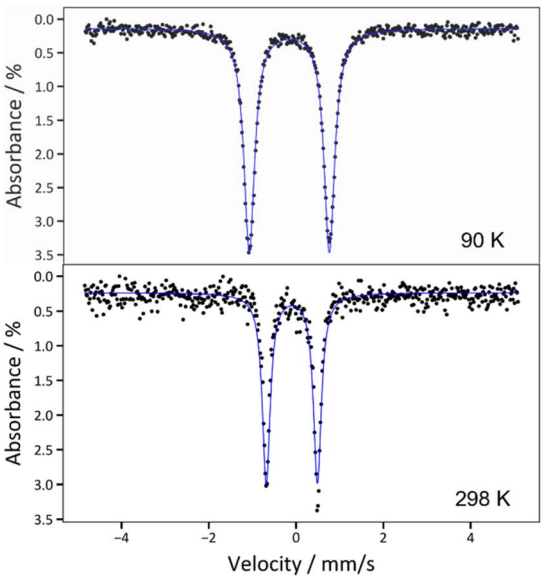

Fig. 3 Zero-field ^{57}Fe Mössbauer spectra of **2** collected at T = 90 K (top) and T = 298 K (bottom). The blue traces correspond to the overall fits, which are described in the main text.

Table 1 Mössbauer parameters for complexes **1**, **2**, **3**, [Fe(N=C^{t}Bu$_2$)$_4$], and [Fe(MesNCH$_2$CH$_2$NMes)$_2$]. O. S. = Formal Oxidation State

Complex	δ (mm s^{-1})	$\lvert\Delta E_Q\rvert$ (mm s^{-1})	O. S.	Ref.
1	0.924(2)	3.537(4)	2	This work
2 (90 K)	−0.162(2)	1.837(3)	4	This work
2 (298 K)	−0.096(4)	1.172(7)	4	This work
3	0.256(2)	0.864(4)	3	52
[Fe(N=C^{t}Bu$_2$)$_4$]	−0.15	1.62	4	48
[Fe(MesNCH$_2$CH$_2$NMes)$_2$]	−0.15	3.00	4	33

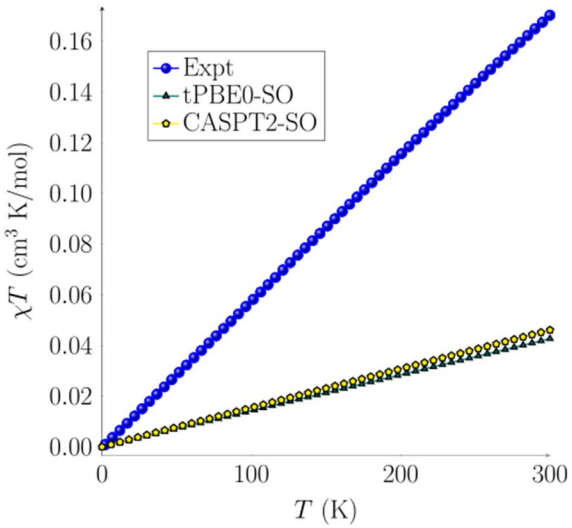

Fig. 4 Magnetic susceptibility plot for complex **2** using TPSSh-D3BJ/def2-TZV optimized structures. Experimental data are shown in blue circles, CASPT2-SO (4, 10) yellow pentagons, and tPBE0-SO (4, 10) green triangles. Experimental data were collected under an applied magnetic field of H = 1k Oe from T = 2 to T = 300 K.

In an effort to explain the spectroscopic and magnetic properties of complex **2**, we performed an extensive computational investigation of its electronic structure using DFT and *ab initio* methods. Computational modeling was performed on the structure extracted from the crystal packing. Geometry optimization considering the singlet (S = 0), triplet (S = 1), and quintet (S = 2) spin states was performed with Kohn–Sham DFT using the functionals TPSSh-D3BJ,[62–64] B3LYP-D3BJ,[65–67] and M06[68] together with def2-TZVP[69] as the basis set for all the atoms. The Gaussian 16 rev. A03 software package[70] was used for all DFT calculations (see the ESI† for full details). The functional TPSSh-D3BJ, which well describes the first–row transition metals including Fe-complexes,[71] in agreement with the previous literature[72,73] and with experiments, was chosen to carry out further DFT calculations (more details in the ESI†).

Structural optimization provides similar singlet and triplet geometries, which suggests that the structures have similar energy. For all the functionals tested here, the root means square deviation (RMSD) between the crystal structure and both the singlet and the triplet optimized geometries is minimal. The RMSD values are between 0.05 Å and 0.32 Å, and the RMDS between the singlet and triplet optimized structures is about 0.25 Å (see the ESI† for additional details).

Energetically, a singlet ground state was obtained using the selected functional TPSSh-D3BJ. The singlet–triplet gap is small with a value of 0.03 eV, which agrees with a low-lying triplet state as suggested experimentally. In contrast, the non-optimized geometry extracted from the crystal structure provides a singlet–triplet gap of about 0.5 eV, which cannot be referred to as a low-lying in character. Therefore, this structure is unsuitable for computing the net singlet or triplet state properties.

To better understand the variable temperature magnetism behavior of complex **2**, complete active space self-consistent field (CASSCF)[74] followed by perturbation theory (CASPT2)[75] and pair-density functional theory (MC-PDFT with the tPBE and tPBE0 functionals)[76,77] calculations were performed. These multireference calculations employed both the 100 K X-ray structure, in which only the hydrogen positions were optimized at the DFT level (discussed in the ESI†) and the TPSSh-D3BJ fully optimized structures previously discussed.

The CASSCF calculations were performed using the state average formalism (SA-CASSCF). From the optimized CASSCF wavefunction, CASPT2 and tPBE0 calculations were performed to obtain the singlet–triplet energy gap and the magnetic susceptibility in three selected active spaces (see the ESI† for computational details). Multireference calculations were also shown to be effective in rationalizing the electronic structure of the Fe(IV) nitride, [Cp′Fe(μ-N)]$_2$ (Cp′ = 1,2,4-^{t}Bu$_3$C$_5$H$_2$), which was not well described by DFT methods.[78]

The active spaces were chosen based on the occupation of the 3d frontier orbitals of the Fe(IV) center and the four N atoms surrounding it. Indeed, the Fe(IV) center of complex **2** has a 3d^4 electron configuration; thus, the minimal active space considered is 4 electrons in 5 3d-orbitals (4, 5). To provide a more accurate electronic and chemical description, a second d-shell (4d) has been added to allow the correlation of the 4 electrons in 10 orbitals, active space (4, 10). This expansion of the active space is necessary to allow further delocalization of the 3d electrons into the 4d-shell. Furthermore, a (12, 9) active space was also chosen by including four Fe–N bonding orbitals to describe the high degree of covalency of metal–ketimide bonds (see ESI† for more details). Indeed, the Fe–N 3d-sp^2 hybrid bonding orbitals allow a further expansion in the direction of the ketimide ligands.[44,45,79] Therefore, such extended active spaces should suffice to explore the physical properties of the system in subsequent calculations. Consistent with the DFT results, CASPT2 predicts a singlet ground state followed by the triplet state, while tPBE0 almost agrees, with a singlet–triplet

Table 2 Calculated relative electronic energies, in eV, between the singlet, triplet, and quintet states. Single point calculations with CASPT2 and tPBE0 with the (4, 10) active space at the TPSSh-D3BJ optimized geometries for **2**

	TPSSh-D3BJ	CASPT2	tPBE0
Singlet	0.00	0.00	0.02
Triplet	0.03	0.11	0.00
Quintet	0.27	2.26	1.84

gap slightly negative; the quintet state lies significantly higher in all methods and is likely not populated to any meaningful extent at the temperatures studied. The singlet–triplet gaps at CASPT2 and tPBE0 are 0.11 eV and −0.02 eV respectively consistent with both states being thermally accessible (Table 2 and the ESI†).

After assessing the different spin states of complex **2**, calculations of its magnetic susceptibility were performed. Spin–orbit coupling (SOC) was computed with the restricted active space state interaction method (RASSI-SO)[80–82] on top of the previously described spin states at both CASPT2-SO and tPBE-SO levels. The spin–orbit energies are reported and discussed in the ESI† (see Tables S12–S14†). The effective spin Hamiltonian for the zero-field parameters and magnetic susceptibility were computed with the SINGLE_ANISO module using OpenMolcas.[83] CASPT2-SO and tPBE0-SO with the (4, 10) active space magnetic susceptibility values are reported in Fig. 4. A total of 5 quintets, 35 triplets, and 22 singlets roots were calculated for all active spaces. These states were chosen based on an energy cut-off of 40 000 cm^{-1}. We observe a linear behavior of χT over the temperature range. The linear plot confirms a singlet ground state with a low-lying triplet excited state. A pure singlet state (diamagnetic) would have resulted in a horizontal line at $\chi T = 0$, whereas a pure triplet state (paramagnetic) would have resulted in a plateauing curve. The mix of such states provides a straight line with a slope (see the ESI† for more details). The computed χT *vs.* T using tPBE0-SO and CASPT2-SO agree with each other (Fig. 4). However, the computed χ_{calc} values only account for the spin–orbit coupling without thermal contributions; thus they are still below the experimental data but within an acceptable deviation, with a difference of about 0.0004 $cm^3\ mol^{-1}$. The error in χ_{calc} is a consequence of performing the geometry optimization calculations at a temperature of 0 K rather than in the 2–300 K range, thus in the absence of any phonon or thermal bath where a deformation of the geometrical structure and subsequent spin-phonon coupling may take place.

Conclusions

In summary, we report the synthesis of $[Fe^{IV}(N{=}C(^tBu)Ph)_4]$, a rare example of a nearly square planar, Fe(IV) coordination complex. Its +4 oxidation state was confirmed *via* ^{57}Fe Mössbauer spectroscopy. In addition, SQUID magnetometry and VT-NMR spectroscopic studies indicate that this complex features a low-lying excited state. The calculated magnetic susceptibility data also show that a low-lying triplet excited state contributes to the paramagnetic behavior observed for **2**. These properties set **2** apart from its di-*tert*-butyl analogue, $[Fe^{IV}(N{=}C^tBu_2)_4]$. The latter complex is diamagnetic at all temperatures studied, likely due to the better electron donating ability of the di-*tert*-butyl ketimide ligand, which results in a stronger ligand field and better separated ground state. The better donating ability of di-*tert*-butyl ketimide is also supported by the cyclic voltammetry data of both complexes. Overall, this work expands our understanding of Fe(IV) coordination chemistry and better defines the conditions under which ketimides can be used to stabilize high oxidation states.

Data availability

The data supporting this article have been included as part of the ESI.† Crystallographic data for **1** and **2** have been deposited at the Cambridge Structural Database under **1**: CCDC 2254712; **2** (100 K): 2254713; **2** (287 K): 2363649.

Author contributions

PRH and RAL performed the synthesis and characterization. GW oversaw the crystallographic analysis. ASdV, AD, and AS performed the computational analysis. LG and TWH supervised the work. PRH, ASdV, AD, AS, LG, and TWH contributed to the writing and editing of the manuscript.

Conflicts of interest

The authors declare no competing financial interest.

Acknowledgements

PRH, RAL, GW, and TWH thank the National Science Foundation (CHE 2055063) for financial support of this work. The computational work (ASdV, AD, AS, and LG) was supported by the Air Force Office Scientific Research by Grant FA9550-20-1-0360. This research made use of a 400 MHz NMR spectrometer supported in part by the NIH Shared Instrumentation Grant, S10OD012077. The MRL Shared Experimental Facilities are supported by the MRSEC Program of the National Science Foundation under award NSF DMR 1720256, a member of the NSF-funded Materials Research Facilities Network. The authors acknowledge the University of Chicago Research Computing Center (RCC) for providing computational resources.

Notes and references

1 J. J. Scepaniak, M. D. Fulton, R. P. Bontchev, E. N. Duesler, M. L. Kirk and J. M. Smith, *J. Am. Chem. Soc.*, 2008, **130**, 10515–10517.
2 J. J. Scepaniak, C. S. Vogel, M. M. Khusniyarov, F. W. Heinemann, K. Meyer and J. M. Smith, *Science*, 2011, **331**, 1049–1052.
3 I. Nieto, F. Ding, R. P. Bontchev, H. Wang and J. M. Smith, *J. Am. Chem. Soc.*, 2008, **130**, 2716–2717.

4 M. P. Mehn and J. C. Peters, *J. Inorg. Biochem.*, 2006, **100**, 634–643.
5 C. M. Thomas, N. P. Mankad and J. C. Peters, *J. Am. Chem. Soc.*, 2006, **128**, 4956–4957.
6 C. V. Sastri, J. Lee, K. Oh, Y. J. Lee, J. Lee, T. A. Jackson, K. Ray, H. Hirao, W. Shin, J. A. Halfen, J. Kim, L. Que, S. Shaik and W. Nam, *Proc. Natl. Acad. Sci. U. S. A.*, 2007, **104**, 19181–19186.
7 C. Vogel, F. W. Heinemann, J. Sutter, C. Anthon and K. Meyer, *Angew. Chem., Int. Ed.*, 2008, **47**, 2681–2684.
8 T. A. Betley and J. C. Peters, *J. Am. Chem. Soc.*, 2004, **126**, 6252–6254.
9 M. S. Vad, A. Lennartson, A. Nielsen, J. Harmer, J. E. McGrady, C. Frandsen, S. Mørup and C. J. McKenzie, *Chem. Commun.*, 2012, **48**, 10880–10882.
10 J. England, J. O. Bigelow, K. M. Van Heuvelen, E. R. Farquhar, M. Martinho, K. K. Meier, J. R. Frisch, E. Münck and L. Que, *Chem. Sci.*, 2014, **5**, 1204–1215.
11 B. P. Jacobs, P. T. Wolczanski, Q. Jiang, T. R. Cundari and S. N. MacMillan, *J. Am. Chem. Soc.*, 2017, **139**, 12145–12148.
12 J.-U. Rohde, J.-H. In, M. H. Lim, W. W. Brennessel, M. R. Bukowski, A. Stubna, E. Münck, W. Nam and L. Que, *Science*, 2003, **299**, 1037–1039.
13 M. R. Bukowski, K. D. Koehntop, A. Stubna, E. L. Bominaar, J. A. Halfen, E. Münck, W. Nam and L. Que, *Science*, 2005, **310**, 1000–1002.
14 J. England, Y. Guo, E. R. Farquhar, V. G. Young Jr, E. Münck and L. Que Jr, *J. Am. Chem. Soc.*, 2010, **132**, 8635–8644.
15 V. F. Oswald, J. L. Lee, S. Biswas, A. C. Weitz, K. Mittra, R. Fan, J. Li, J. Zhao, M. Y. Hu, E. E. Alp, E. L. Bominaar, Y. Guo, M. T. Green, M. P. Hendrich and A. S. Borovik, *J. Am. Chem. Soc.*, 2020, **142**, 11804–11817.
16 D. C. Lacy, R. Gupta, K. L. Stone, J. Greaves, J. W. Ziller, M. P. Hendrich and A. S. Borovik, *J. Am. Chem. Soc.*, 2010, **132**, 12188–12190.
17 J. P. Bigi, W. H. Harman, B. Lassalle-Kaiser, D. M. Robles, T. A. Stich, J. Yano, R. D. Britt and C. J. Chang, *J. Am. Chem. Soc.*, 2012, **134**, 1536–1542.
18 A. K. Maity, J. Murillo, A. J. Metta-Magaña, B. Pinter and S. Fortier, *J. Am. Chem. Soc.*, 2017, **139**, 15691–15700.
19 C. Souilah, S. A. V. Jannuzzi, D. Demirbas, S. Ivlev, M. Swart, S. DeBeer and A. Casitas, *Angew. Chem., Int. Ed.*, 2022, **61**, e202201699.
20 O. Prakash, P. Chábera, N. W. Rosemann, P. Huang, L. Häggström, T. Ericsson, D. Strand, P. Persson, J. Bendix, R. Lomoth and K. Wärnmark, *Chem.–Eur. J.*, 2020, **26**, 12728–12732.
21 A. Casitas, J. A. Rees, R. Goddard, E. Bill, S. DeBeer and A. Fürstner, *Angew. Chem., Int. Ed.*, 2017, **56**, 10108–10113.
22 M. Malischewski, K. Seppelt, J. Sutter, D. Munz and K. Meyer, *Angew. Chem., Int. Ed.*, 2018, **57**, 14597–14601.
23 M. Malischewski, K. Seppelt, J. Sutter, F. W. Heinemann, B. Dittrich and K. Meyer, *Angew. Chem., Int. Ed.*, 2017, **56**, 13372–13376.
24 M. Malischewski, M. Adelhardt, J. Sutter, K. Meyer and K. Seppelt, *Science*, 2016, **353**, 678–682.
25 C. Milsmann, S. Sproules, E. Bill, T. Weyhermüller, S. D. George and K. Wieghardt, *Chem.–Eur. J.*, 2010, **16**, 3628–3645.
26 M. Atanasov, P. Surawatanawong, K. Wieghardt and F. Neese, *Coord. Chem. Rev.*, 2013, **257**, 27–41.
27 R. A. Lewis, G. Wu and T. W. Hayton, *J. Am. Chem. Soc.*, 2010, **132**, 12814–12816.
28 B. K. Bower and H. G. Tennent, *J. Am. Chem. Soc.*, 1972, **94**, 2512–2514.
29 C. C. Cummins and R. R. Schrock, *Inorg. Chem.*, 1994, **33**, 395–396.
30 A. Chanda, D.-L. Popescu, F. T. de Oliveira, E. L. Bominaar, A. D. Ryabov, E. Münck and T. J. Collins, *J. Inorg. Biochem.*, 2006, **100**, 606–619.
31 J. England, E. R. Farquhar, Y. Guo, M. A. Cranswick, K. Ray, E. Münck and L. Que Jr, *Inorg. Chem.*, 2011, **50**, 2885–2896.
32 J. H. Lim, X. Engelmann, S. Corby, R. Ganguly, K. Ray and H. S. Soo, *Chem. Sci.*, 2018, **9**, 3992–4002.
33 B. Zhang, J. P. Joyce, N. Wolford, W. W. Brennessel, S. DeBeer and M. Neidig, *Angew. Chem., Int. Ed.*, 2024, **63**, e202405113.
34 T. J. Collins, K. L. Kostka, E. S. Uffelman and T. L. Weinberger, *Inorg. Chem.*, 1991, **30**, 4204–4210.
35 T. J. Collins, *Acc. Chem. Res.*, 1994, **27**, 279–285.
36 T. Kojima, F. Ogishima, T. Nishibu, H. Kotani, T. Ishizuka, T. Okajima, S. Nozawa, Y. Shiota, K. Yoshizawa, H. Ohtsu, M. Kawano, T. Shiga and H. Oshio, *Inorg. Chem.*, 2018, **57**, 9683–9695.
37 A. Ikezaki, M. Takahashi and M. Nakamura, *Chem. Commun.*, 2013, **49**, 3098–3100.
38 Y. Morimoto, Y. Shimaoka, Y. Ishimizu, H. Fujii and S. Itoh, *Angew. Chem., Int. Ed.*, 2019, **58**, 10863–10866.
39 H. Li, L. Wang, Y. Hu, Z. Zhang, D. Wan, Q. Fan, R. B. King and H. F. Schaefer III, *J. Phys. Chem. A*, 2020, **124**, 6867–6876.
40 D. J. Liptrot, J.-D. Guo, S. Nagase and P. P. Power, *Angew. Chem., Int. Ed.*, 2016, **55**, 14766–14769.
41 D. J. Liptrot and P. P. Power, *Nat. Rev. Chem.*, 2017, **1**, 0004.
42 H. Li, Y. Hu, D. Wan, Z. Zhang, Q. Fan, R. B. King and H. F. Schaefer III, *J. Phys. Chem. A*, 2019, **123**, 9514–9519.
43 C. R. Graves, A. E. Vaughn, E. J. Schelter, B. L. Scott, J. D. Thompson, D. E. Morris and J. L. Kiplinger, *Inorg. Chem.*, 2008, **47**, 11879–11891.
44 R. A. Lewis, S. P. George, A. Chapovetsky, G. Wu, J. S. Figueroa and T. W. Hayton, *Chem. Commun.*, 2013, **49**, 2888–2890.
45 P. L. Damon, C. J. Liss, R. A. Lewis, S. Morochnik, D. E. Szpunar, J. Telser and T. W. Hayton, *Inorg. Chem.*, 2015, **54**, 10081–10095.
46 A. M. Martins, M. M. Marques, J. R. Ascenso, A. R. Dias, M. T. Duarte, A. C. Fernandes, S. Fernandes, M. J. Ferreira, I. Matos, M. Conceição Oliveira, S. S. Rodrigues and C. Wilson, *J. Organomet. Chem.*, 2005, **690**, 874–884.
47 R. A. Lewis, G. Wu and T. W. Hayton, *Inorg. Chem.*, 2011, **50**, 4660–4668.
48 R. A. Lewis, D. E. Smiles, J. M. Darmon, S. C. E. Stieber, G. Wu and T. W. Hayton, *Inorg. Chem.*, 2013, **52**, 8218–8227.

49 R. A. D. Soriaga, J. M. Nguyen, T. A. Albright and D. M. Hoffman, *J. Am. Chem. Soc.*, 2010, **132**, 18014–18016.
50 L. A. Seaman, G. Wu, N. Edelstein, W. W. Lukens, N. Magnani and T. W. Hayton, *J. Am. Chem. Soc.*, 2012, **134**, 4931–4940.
51 M. K. Assefa, D.-C. Sergentu, L. A. Seaman, G. Wu, J. Autschbach and T. W. Hayton, *Inorg. Chem.*, 2019, **58**, 12654–12661.
52 P. R. Hertler, R. A. Lewis, G. Wu and T. W. Hayton, *Inorg. Chem.*, 2023, **62**, 11829–11836.
53 L. Yang, D. R. Powell and R. P. Houser, *Dalton Trans.*, 2007, 955–964.
54 A. Bondi, *J. Phys. Chem.*, 1964, **68**, 441–451.
55 S. C. Bart, K. Chłopek, E. Bill, M. W. Bouwkamp, E. Lobkovsky, F. Neese, K. Wieghardt and P. J. Chirik, *J. Am. Chem. Soc.*, 2006, **128**, 13901–13912.
56 L. A. Abriata, G. N. Ledesma, R. Pierattelli and A. J. Vila, *J. Am. Chem. Soc.*, 2009, **131**, 1939–1946.
57 N. V. Shokhirev and F. A. Walker, *J. Phys. Chem.*, 1995, **99**, 17795–17804.
58 C. Hansch, A. Leo and R. W. Taft, *Chem. Rev.*, 1991, **91**, 165–195.
59 M. P. Hendrich, W. Gunderson, R. K. Behan, M. T. Green, M. P. Mehn, T. A. Betley, C. C. Lu and J. C. Peters, *Proc. Natl. Acad. Sci. U. S. A.*, 2006, **103**, 17107–17112.
60 P. Gütlich, E. Bill and A. X. Trautwein, in *Mössbauer Spectroscopy and Transition Metal Chemistry: Fundamentals and Applications*, ed. P. Gütlich, E. Bill and A. X. Trautwein, Springer Berlin Heidelberg, Berlin, Heidelberg, 2011, pp. 73–135.
61 J. Li, B. C. Noll, A. G. Oliver, C. E. Schulz and W. R. Scheidt, *J. Am. Chem. Soc.*, 2013, **135**, 15627–15641.
62 J. Tao, J. P. Perdew, V. N. Staroverov and G. E. Scuseria, *Phys. Rev. Lett.*, 2003, **91**, 146401.
63 V. N. Staroverov, G. E. Scuseria, J. Tao and J. P. Perdew, *J. Chem. Phys.*, 2003, **119**, 12129–12137.
64 S. Grimme, S. Ehrlich and L. Goerigk, *J. Comp. Chem.*, 2011, **32**, 1456–1465.
65 A. D. Becke, *J. Chem. Phys.*, 1992, **96**, 2155–2160.
66 C. Lee, W. Yang and R. G. Parr, *Phys. Rev. B*, 1988, **37**, 785–789.
67 S. H. Vosko, L. Wilk and M. Nusair, *Can. J. Phys.*, 1980, **58**, 1200–1211.
68 Y. Zhao and D. G. Truhlar, *Theor. Chem. Acc.*, 2008, **120**, 215–241.
69 F. Weigend and R. Ahlrichs, *Phys. Chem. Chem. Phys.*, 2005, **7**, 3297–3305.
70 M. J. Frisch, G. W. Trucks, H. B. Schlegel, G. E. Scuseria, M. A. Robb, J. R. Cheeseman, G. Scalmani, V. Barone, G. A. Petersson, H. Nakatsuji, X. Li, M. Caricato, A. V. Marenich, J. Bloino, B. G. Janesko, R. Gomperts, B. Mennucci, H. P. Hratchian, J. V. Ortiz, A. F. Izmaylov, J. L. Sonnenberg, D. Williams-Young, F. Ding, F. Lipparini, F. Egidi, J. Goings, B. Peng, A. Petrone, T. Henderson, D. Ranasinghe, V. G. Zakrzewski, J. Gao, N. Rega, G. Zheng, W. Liang, M. Hada, M. Ehara, K. Toyota, R. Fukuda, J. Hasegawa, M. Ishida, T. Nakajima, Y. Honda, O. Kitao, H. Nakai, T. Vreven, K. Throssell, J. A. Montgomery Jr, J. E. Peralta, F. Ogliaro, M. J. Bearpark, J. J. Heyd, E. N. Brothers, K. N. Kudin, V. N. Staroverov, T. A. Keith, R. Kobayashi, J. Normand, K. Raghavachari, A. P. Rendell, J. C. Burant, S. S. Iyengar, J. Tomasi, M. Cossi, J. M. Millam, M. Klene, C. Adamo, R. Cammi, J. W. Ochterski, R. L. Martin, K. Morokuma, O. Farkas, J. B. Foresman and D. J. Fox, *Gaussian 16, Revision A.03*, Wallingford, CT, 2016.
71 K. P. Jensen and J. Cirera, *J. Phys. Chem. A*, 2009, **113**, 10033–10039.
72 A. Darù, C. Martín-Fernández and J. N. Harvey, *ACS Catal.*, 2022, **12**, 12678–12688.
73 N. Jiang, A. Darù, Š. Kunstelj, J. G. Vitillo, M. E. Czaikowski, A. S. Filatov, A. Wuttig, L. Gagliardi and J. S. Anderson, *J. Am. Chem. Soc.*, 2024, **146**, 12243–12252.
74 B. O. Roos, in *Advances in Chemical Physics*, 1987, pp. 399–445.
75 K. Andersson, P. Å. Malmqvist and B. O. Roos, *J. Chem. Phys.*, 1992, **96**, 1218–1226.
76 G. Li Manni, R. K. Carlson, S. Luo, D. Ma, J. Olsen, D. G. Truhlar and L. Gagliardi, *J. Chem. Theory Comput.*, 2014, **10**, 3669–3680.
77 R. Pandharkar, M. R. Hermes, D. G. Truhlar and L. Gagliardi, *J. Phys. Chem. Lett.*, 2020, **11**, 10158–10163.
78 M. Reiners, M. Maekawa, C. G. Daniliuc, M. Freytag, P. G. Jones, P. S. White, J. Hohenberger, J. Sutter, K. Meyer, L. Maron and M. D. Walter, *Chem. Sci.*, 2017, **8**, 4108–4122.
79 A. W. Cook, P. Hrobárik, P. L. Damon, D. Najera, B. Horváth, G. Wu and T. W. Hayton, *Inorg. Chem.*, 2019, **58**, 15927–15935.
80 B. O. Roos and P.-Å. Malmqvist, *Phys. Chem. Chem. Phys.*, 2004, **6**, 2919–2927.
81 B. A. Heß, C. M. Marian, U. Wahlgren and O. Gropen, *Chem. Phys. Lett.*, 1996, **251**, 365–371.
82 P. Å. Malmqvist, B. O. Roos and B. Schimmelpfennig, *Chem. Phys. Lett.*, 2002, **357**, 230–240.
83 G. Li Manni, I. Fdez. Galván, A. Alavi, F. Aleotti, F. Aquilante, J. Autschbach, D. Avagliano, A. Baiardi, J. J. Bao, S. Battaglia, L. Birnoschi, A. Blanco-González, S. I. Bokarev, R. Broer, R. Cacciari, P. B. Calio, R. K. Carlson, R. Carvalho Couto, L. Cerdán, L. F. Chibotaru, N. F. Chilton, J. R. Church, I. Conti, S. Coriani, J. Cuéllar-Zuquin, R. E. Daoud, N. Dattani, P. Decleva, C. de Graaf, M. G. Delcey, L. De Vico, W. Dobrautz, S. S. Dong, R. Feng, N. Ferré, M. Filatov, L. Gagliardi, M. Garavelli, L. González, Y. Guan, M. Guo, M. R. Hennefarth, M. R. Hermes, C. E. Hoyer, M. Huix-Rotllant, V. K. Jaiswal, A. Kaiser, D. S. Kaliakin, M. Khamesian, D. S. King, V. Kochetov, M. Krośnicki, A. A. Kumaar, E. D. Larsson, S. Lehtola, M.-B. Lepetit, H. Lischka, P. López Ríos, M. Lundberg, D. Ma, S. Mai, P. Marquetand, I. C. D. Merritt, F. Montorsi, M. Mörchen,

A. Nenov, V. H. A. Nguyen, Y. Nishimoto, M. S. Oakley, M. Olivucci, M. Oppel, D. Padula, R. Pandharkar, Q. M. Phung, F. Plasser, G. Raggi, E. Rebolini, M. Reiher, I. Rivalta, D. Roca-Sanjuán, T. Romig, A. A. Safari, A. Sánchez-Mansilla, A. M. Sand, I. Schapiro, T. R. Scott, J. Segarra-Martí, F. Segatta, D.-C. Sergentu, P. Sharma, R. Shepard, Y. Shu, J. K. Staab, T. P. Straatsma, L. K. Sørensen, B. N. C. Tenorio, D. G. Truhlar, L. Ungur, M. Vacher, V. Veryazov, T. A. Voß, O. Weser, D. Wu, X. Yang, D. Yarkony, C. Zhou, J. P. Zobel and R. Lindh, *J. Chem. Theory Comput.*, 2023, **19**, 6933–6991.